Coupling Character between Imidazole and Imidazole Cation: Implication for the Coupling Modes of Biomolecular Residues

Shihai Yan,[†] Yuxiang Bu,*[,†,‡] Zhaohua Cao,[†] and Ping Li[†,‡]

Key Laboratory of Colloid and Interface Chemistry of the Ministry of Education, Institute of Theoretical Chemistry, Shandong University, Jinan, 250100, P. R. China, and Department of Chemistry, Qufu Normal University, Qufu, 273165, P. R. China

Received: April 2, 2004; In Final Form: June 17, 2004

On the basis of the reliable B3LYP/6-311+G* method, four kinds of coupling modes for the complexes of imidazole and imidazole cation are found through the geometry optimizations. In total, 19 stable complexes are found on the global potential energy surfaces, and they may be classified as: C···N mode, N···N mode, single H-bond mode, and double H-bond mode. The harmonic vibrational frequency, charge population, and spin density analyses are carried out, and the coupling character of each complex is analyzed. Optimizations have indicated the spontaneous proton transfers between two moieties of each complex that includes the N−H···N type H-bond. The relative stability after the BSSE and ZPE corrections is compared, and the most stable complexes are those with N−H···N type H-bonds. The calculated adiabatic electron affinities, E_A, of these complexes are near 180.0 kcal/mol, and the E_A of the complex with the linear C−H···N type H-bond is the biggest while that with proton transfer is the smallest. The difference of the E_As and vertical E_As (VE_As) and their origins are compared. The deformation energies of the C···N covalent mode complexes are larger while those of the double H-bond mode complexes are smaller. Preliminary analyses indicate that there are many possible interaction modes among different biological fragments and the different coupling modes may yield different effect on the biomolecule structures and further regulate their functionality and reactivity mechanism.

1. Introduction

The imidazole ($N_2C_3H_4$) molecule, an azole with two virtually identical nitrogens in the ring, is of fundamental importance since its ring is a vital constituent in biological structures,[1] where it is involved in electron transfer in photosynthesis, nucleic acid bases, and amino acids, specifically, enzyme action and protein structural determination.[2−4] On the other hand, the widespread occurrence and importance of hydrogen bonds have made them an active topic. The unique ring structure of imidazole permits the proton to be picked up by one N atom and the other H/H^+ to be released from the other N atom. This action has been proposed to explain the proton conductivity properties[5] of imidazole in the solid state and also in the actual biological surrounding where a long H-bonded chain is present.

Accordingly, experimental[5−10] and theoretical[11−16] studies have been applied to the investigations of the properties of imidazole and its ramifications. The study about imidazole is more active in recent years. In the experiment fields, the protonic conductivity in imidazole single crystal has been studied,[5] and it has been pointed out that the rate-determining step is reorientation and the conductivity in imidazole crystals is due to proton transfer. Crystalline imidazole has been studied for its vibrations and intra- and intermolecular force constants.[6,7] The vibrational modes of imidazole in solid state have been assigned in ref 7. High-pressure infrared spectroscopy is used in probing the C−H−O interactions in the protonated imidazole aqueous solution.[8] For the theoretical studies, some low-lying electronic states of imidazole and the proton-transfer shuttling with stationary and mobile imidazole have also been investigated in detail.[12,13] The interactions of imidazole with other biological system[14] and imidazolium[15] and the cation binding effect on hydrogen bonding[16] have been explored.

Although the importance of imidazole has intrigued many researchers, the investigations of this are still deficient. Studies about the interaction of the imidazole molecule might provide nonnegligible contributions to the protein structure and the enzyme mechanisms in biological systems. Therefore, in this work, we will focus on the coupling modes of imidazole and imidazole cation using a quantum chemistry method to explore its coupling properties and the mechanisms associated with relevant processes. The geometries, the harmonic vibrational frequencies, atomic charge population, the spin density distribution, the relative stability with zero point vibrational energy (ZPE) correction and the basis set superposition error (BSSE)[17] correction, and the adiabatic and vertical electron affinities are discussed, and some interesting observations and characters are analyzed.

2. Computational Details

Density functional theory and ab initio calculations have been performed using the Gaussian 98 program.[18] At first, the imidazole (Im) geometry is optimized using MP2 and B3LYP methods at the 6-311+G* and 6-311++G** basis set levels. Then, the complexes (Im^+···Im) formed by Im and imidazole cation (Im^+) radical are optimized at the B3LYP/6-311+G*

* Corresponding author. Institute of Theoretical Chemistry, Shandong University, Jinan, 250100, P. R. China. Telephone: 86-531-8365740. Fax: 86-531-8564464. E-mail: byx@sdu.edu.cn.

[†] Shandong University.

[‡] Qufu Normal University.

10.1021/jp048549y CCC: $27.50
Published on Web 08/04/2004

TABLE 1: Optimized Geometry Parameters (Bond Length in Å; Bond Angle in deg) of Im Using B3LYP and MP2 Methods

	B3LYP		MP2			
	6-311 +G*	6-311 ++G**	6-311 +G*	6-311 ++G**	others[7]	expt[9]
R(1,2)	1.312	1.312	1.325	1.325	1.312	1.364
R(1,3)	1.367	1.367	1.367	1.367	1.363	1.314
R(1,6)	1.080	1.079	1.081	1.081	1.077	1.079
R(2,4)	1.377	1.377	1.377	1.377	1.381	1.382
R(3,5)	1.380	1.380	1.376	1.376	1.376	1.377
R(3,7)	1.008	1.008	1.009	1.010	0.991	0.998
R(4,5)	1.370	1.371	1.382	1.382	1.362	1.364
R(4,8)	1.080	1.079	1.081	1.081	1.070	1.078
R(5,9)	1.078	1.077	1.080	1.079	1.071	1.078
A(2,1,3)	111.6	111.5	111.6	111.6	112.0	112.0
A(1,2,4)	105.5	105.5	105.0	105.1	104.9	104.9
A(1,3,5)	107.1	107.2	107.5	107.5	106.9	106.9
A(2,4,5)	110.6	110.6	110.8	110.9	110.7	110.7
A(3,5,4)	105.1	105.1	105.0	104.9	105.5	105.5

TABLE 2: Frequencies (in cm^{-1}) and IR Intensities (KM/mol) of Im and Im^+ Cation Obtained at the B3LYP/6-311+G* Level

	Im		Im^+	
	freq	IR intens	freq	IR intens
A″	507.2	102.2	487.3	26.2
A″	641.6	11.1	539.8	8.9
A″	679.2	6.6	707.9	144.3
A″	716.4	45.1	785.0	0.1
A″	799.6	43.3	825.8	7.2
A″	858.1	6.3	864.7	1.7
A′	909.3	6.8	906.2	2.1
A′	946.6	2.2	923.5	1.9
A′	1073.8	40.4	965.4	14.7
A′	1096.5	22.1	1043.9	14.6
A′	1147.8	3.9	1128.6	46.1
A′	1160.8	5.0	1212.7	14.1
A′	1285.7	0.5	1268.9	37.6
A′	1366.2	6.8	1293.2	3.9
A′	1437.2	17.0	1421.6	28.5
A′	1501.5	21.9	1460.2	97.6
A′	1562.3	13.1	1452.9	25.7
A′	3241.5	6.9	3248.4	18.8
A′	3246.6	1.7	3257.4	39.3
A′	3271.3	2.7	3262.9	0.5
A′	3654.5	42.4	3580.4	187.8

TABLE 3: Mulliken Charge Populations (*Q*) and Spin Densities (ρ) of the Monomers Determined at the B3LYP/6-311+G* Basis Set Level

	Im	Im^+	
atoms	*Q*	*Q*	ρ
C_1	−0.169	−0.078	0.451
N_2	−0.159	−0.023	−0.102
N_3	−0.275	−0.212	−0.078
C_4	−0.199	−0.076	0.320
C_5	−0.263	−0.091	0.472
H_6	0.222	0.330	−0.024
H_7	0.398	0.486	0.001
H_8	0.218	0.327	−0.017
H_9	0.226	0.337	−0.022

level. To investigate the proton-transfer processes, the relaxed potential energy surface (PES) scan calculations are performed at the same level along the N−H···N axis. Vibrational frequency analysis for each configuration is also performed to verify whether the optimized structures correspond to the true local minima on the global PES. The zero-point vibrational energies (ZPE) are obtained and used as a correction in calculations of the relative thermodynamic stabilization energies (E_s) of the optimized configurations. In the calculations of E_s, the effect of the basis set superposition error (BSSE) has also been considered using the counterpoise correction method, but the influence on results is comparative slightly. The optimized

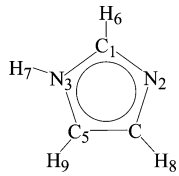

Figure 1. Framework and the numbering of neutral and cation imidazoles.

equilibrium $Im^+\cdots Im$ is used as the starting structure in the optimizations of the neutral complexes, and these optimizations are performed using the B3LYP method employing the 6-311+G* basis set in order to generate the geometries and the energies of the corresponding neutral complexes for the determinations of the adiabatic electron affinities (E_A). The ZPE correction is considered in the calculations of E_A. Similarly, the vertical electron affinities (VE_A) of the $Im^+\cdots Im$ have also been determined as a comparison with the E_A. The adiabatic electron affinities are computed as the difference between the absolute energies of the cation and neutral species at their respective optimized geometries. The vertical electron affinities are calculated as the difference between the absolute energies of the cation and neutral species at the optimized cation geometries. The E_A and VE_A are obtained from the following relations.

$$E_A = E_{(\text{optimized cation})} - E_{(\text{optimized neutral})}$$

$$VE_A = E_{(\text{optimized cation})} - E_{(\text{neutral at optimized cation geometry})}$$

A positive E_A implies that the neutral is lower in energy than the corresponding cation parent molecule and hence stable. The difference of E_A and VE_A implies the deviation of the neutral complex at the optimized cation geometry from the corresponding optimized neutral one.

3. Results and Discussion

To examine the applicability of the theoretical methods, taking the imidazole molecule as an example, the geometry has been optimized using MP2 and B3LYP methods at 6-311+G* and 6-311++G** basis set levels, and the geometrical parameters are compared with the experimental values. Good agreement has been found among them, indicating that the B3LYP/6-311+G* method is reliable and more suitable for these systems. In addition, considering of the cost of CPU time,[19] the B3LYP/6-311+G* method is employed through all calculations. The calculated results and the experimental data are given in Tables 1−3. The corresponding atomic serial numbering of imidazole is depicted in Figure 1, and the numbering rule is also applicable to the complexes.

The geometry optimizations of the complexes have been carried out at B3LYP/6-311+G* level for the complexes formed by Im and Im^+. Four interesting coupling modes have been found in the optimizations, and they may be classified as follows: (1) C···N coupling mode, (2) N···N coupling mode, (3) single H-bond mode, and (4) double H-bond mode. The C···N coupling mode consists of the C−N covalent bond (1A) and the C···N weak interaction (1B) modes. The N···N coupling mode includes the folding (2A) and the collinear (2B) modes. The single H-bond mode can be divided into two types, which are the C−H···N (3A) and the N−H···N (3B) modes. The double H-bond mode is denoted with a 4, and there are three different complexes which involve two H-bonds. These complexes are denoted as 1A1, 1A2, 1A3, 1A4, 1B1, 1B2, 2A1, 2A2, 2B1, 2B2, 3A1, 3A2, 3A3, 3A4, 3B1, 3B2, 4A, 4B, and 4C in short, respectively. These optimized geometries of the

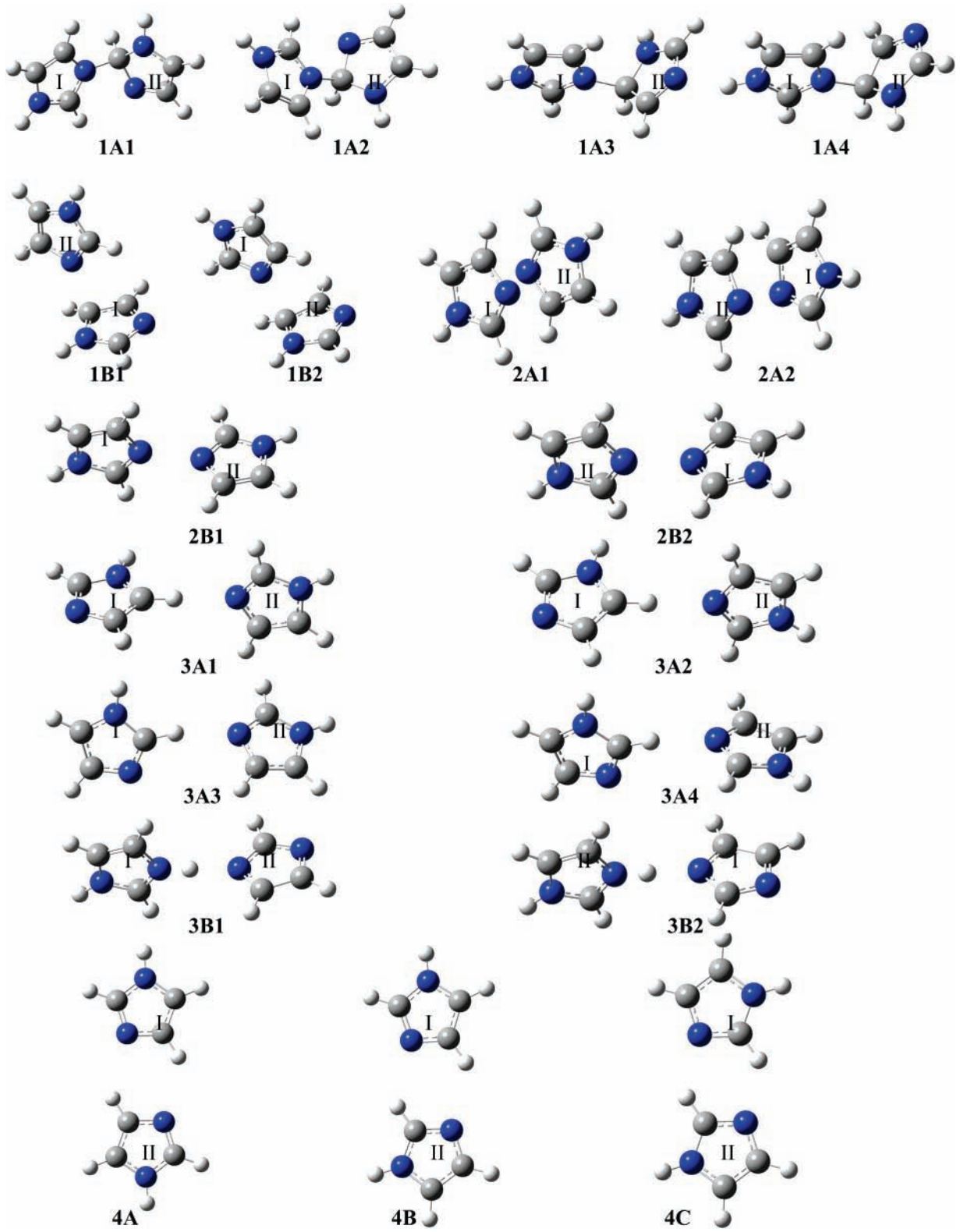

Figure 2. Optimized geometry structures of the complexes at the B3LYP/6-311+G* level.

$Im\cdots Im^+$ complexes are all collected in Figure 2. In this figure, **I** and **II** denote the first and the second fragments (the rings) of the complexes, respectively. The harmonic vibrational IR spectra of the complexes are displayed in Figures 3−5 and 7, respectively. The primary vibrational modes have been assigned in the figures. Figure 6 shows the shape of the potential energy curves for the proton-transfer processes. The Mulliken charge populations (Q) and spin densities (ρ) distribution of the complexes are calculated for its importance in understanding organic radicals. In particular, the ρ distribution is helpful in analyzing the structures of the compounds and useful in judging which part is oxidized. Therefore, in Tables 4−7, the Mulliken charge populations (Q) and the spin densities (ρ) of the complexes obtained at B3LYP/6-311+G* level are collected, respectively. The theoretical dipole moments (DM) and the stabilization energies (E_s) of the complexes are given in Table 8. The stabilization energies are corrected with ZPE and the counterpoise correction method for BSSE. In Figure 8, the

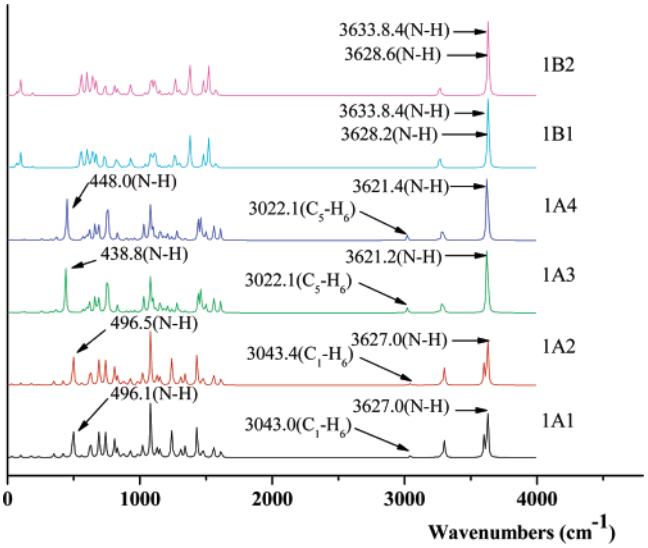

Figure 3. IR spectra of the C−N coupling mode obtained at the B3LYP/6-311+G* level.

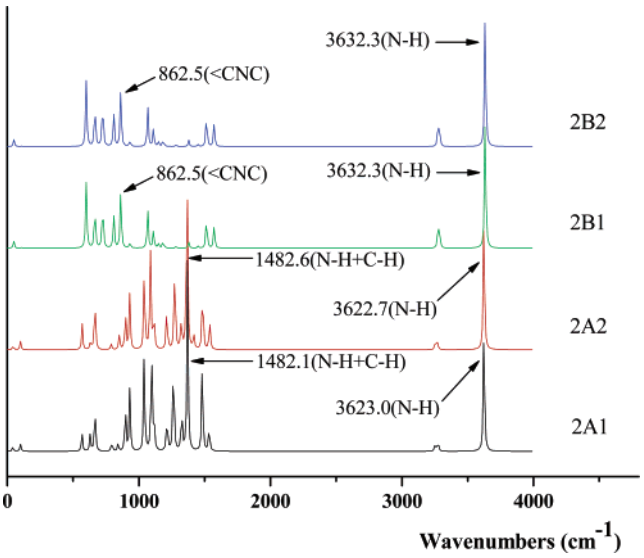

Figure 4. IR spectra of the N−N coupling mode obtained at the B3LYP/6-311+G* level.

relative energies of the optimized cation and neutral complexes, the adiabatic (E_A) and the vertical (VE_A) electron affinities of the complexes, calculated at the same level are collected. In the following sections, the discussions are performed according to the coupling modes.

3.1. C···N Mode. From Figure 2 it can be seen clearly that the C···N mode consists of two typical (covalent and weak interaction) coupling modes. For the C···N covalent one, four stable complexes, 1A1, 1A2, 1A3, and 1A4, are found. Only two complexes, 1B1 and 1B2, are found for the C···N weak coupling mode. The most distinct characteristic of the covalent mode is that two fragments contact directly with each other via an actual covalent bond (C−N covalent bond), while the characteristic of the weak interaction mode is that two fragments interact mainly through the van der Waals force; therefore, the combination is weak, and the contact distance is long.

The C−N covalent coupling mode includes four complexes. The N_2 atom of **I** contacts with the C_1 atom of **II** directly, forming a novel stable complex, 1A1. The bond length of N_2(**I**)−C_1(**II**) is only 1.518 Å, a little longer than the bond length of the common C−N single bond (∼1.47 Å) at the same level.

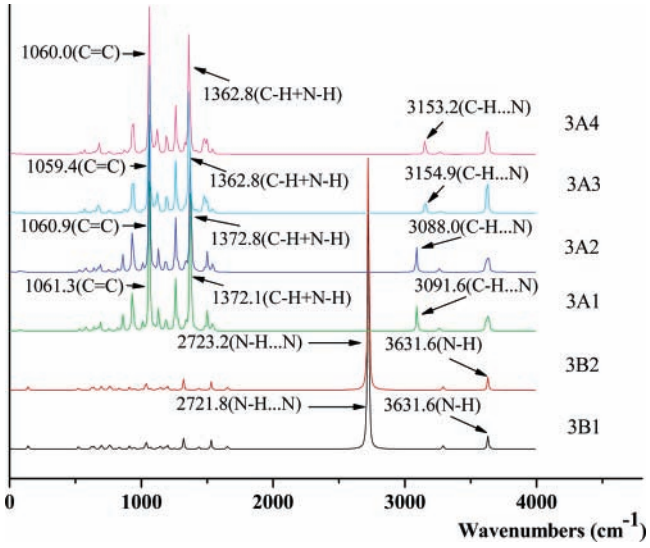

Figure 5. IR spectra of the single H-bond coupling mode obtained at the B3LYP/6-311+G* level.

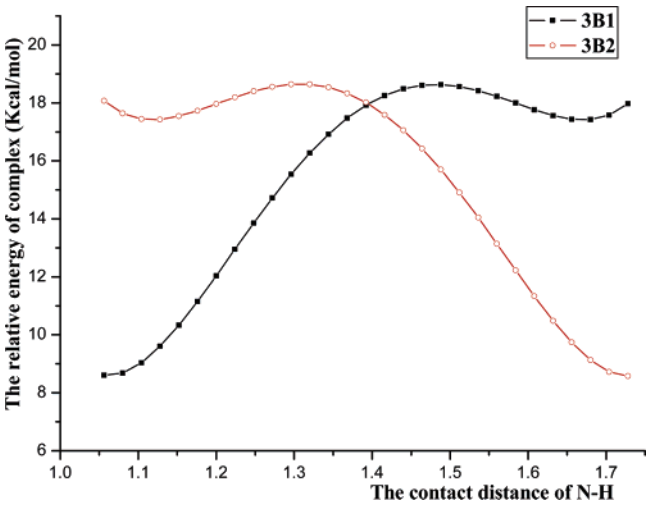

Figure 6. Proton-transfer potential energy surfaces (PES) of 3B1 and 3B2 complexes obtained at the B3LYP/6-311+G* level. The *X*-coordinate refers to contact distance of N(**I**)−H of the N−H···N mode. The *Y*-coordinate refers to the relative energies of 3B1 and 3B2 to the same zero point.

The C_1(**II**) atom is almost in the plane of **I**, while the H_6(**II**) atom is out of the plane of **II** any more for strong local handicap and charge repulsion brought from **I** species. The angle ∠N_2(**I**)−C_1(**II**)−H_6(**II**) is 105.5°. The structure of 1A2 can be obtained if **I** and **II** moieties of 1A1 rotate around N_2(**I**)−C_1(**II**) bond by 180°, respectively. The N_2(**I**)−C_1(**II**) bond length and the ∠N_2(**I**)−C_1(**II**)−H_6(**II**) angle are equal to those of 1A1, respectively. For the same reason with 1A1, the C_1(**II**) is almost in the plane of **I** while the H_6(**II**) is out of the plane of **II** any more. Therefore, it can be drawn that the effect of the rotation brought to 1A1 is weaker. In the structure of 1A3, the N_2 atom of **I** interacts directly with the C_5(**II**) atom. The bond length of N_2(**I**)−C_5(**II**) is 1.533 Å, a little longer compared with the N_2(**I**)−C_1(**II**) bond of 1A1. Thus, it can be inferred that the effect of **I** on **II** for 1A3 should be weaker compared with 1A1. This can be verified by the angle of ∠N_2(**I**)−C_5(**II**)−H_6(**II**) (103.6°), smaller compared with the corresponding angle of 1A1 (105.5°). The angles of ∠N_2(**I**)−C_5(**II**)−N_3(**II**) and ∠N_2(**I**)−C_5(**II**)−H_4(**II**) of 1A3 are 111.5° and 112.1°, respectively. The coupling mode of 1A4 is similar to that of 1A3, and N_2(**I**) also contacts with C_5(**II**) directly, and the corresponding bond length of N_2-

TABLE 4: Mulliken Charge Populations (*Q*) of the C−N and N−N Modes Complexes Determined at the B3LYP/6-311+G* Level

	C−N						N−N			
	covalent bond				weak Coupling		folding		collinear	
	1A1	1A2	1A3	1A4	1B1	1B2	2A1	2A2	2B1	2B2
C_1	−0.030	−0.030	−0.040	−0.046	−0.102	−0.100	−0.393	−0.317	−0.172	−0.172
N_2	0.263	0.263	0.369	0.364	−0.032	0.067	0.032	0.000	0.046	0.046
N_3	−0.253	−0.253	−0.221	−0.221	−0.170	−0.224	−0.160	−0.159	−0.231	−0.231
C_4	−0.048	−0.048	0.093	0.090	−0.125	0.147	0.093	0.081	−0.090	−0.090
C_5	−0.362	−0.362	−0.549	−0.542	−0.395	−0.677	−0.380	−0.411	−0.344	−0.344
H_6	0.331	0.331	0.290	0.291	0.290	0.260	0.294	0.286	0.274	0.274
H_7	0.492	0.492	0.488	0.487	0.444	0.460	0.449	0.450	0.467	0.467
H_8	0.273	0.273	0.304	0.304	0.290	0.268	0.271	0.274	0.269	0.269
H_9	0.295	0.296	0.299	0.299	0.303	0.279	0.295	0.296	0.281	0.281
C_1'	−0.777	−0.777	−0.113	−0.115	−0.212	−0.111	−0.393	−0.317	−0.172	−0.172
N_2'	−0.067	−0.067	−0.029	−0.031	0.086	−0.019	0.032	0.000	0.046	0.046
N_3'	−0.192	−0.192	−0.327	−0.334	−0.233	−0.189	−0.160	−0.159	−0.231	−0.231
C_4'	−0.073	−0.073	−0.241	−0.240	0.053	−0.149	0.093	0.081	−0.090	−0.090
C_5'	−0.118	−0.118	−0.530	−0.516	−0.467	−0.336	−0.380	−0.411	−0.344	−0.344
H_6'	0.317	0.317	0.269	0.270	0.271	0.291	0.294	0.286	0.274	0.274
H_7'	0.402	0.402	0.403	0.405	0.465	0.445	0.449	0.450	0.467	0.467
H_8'	0.269	0.269	0.263	0.262	0.256	0.290	0.271	0.274	0.269	0.269
H_9'	0.279	0.279	0.272	0.272	0.279	0.298	0.295	0.296	0.281	0.281

TABLE 5: Spin Densities (ρ) over the Backbone Atoms of the C−N and N−N Mode Complexes Obtained at B3LYP/6-311+G* Level[a]

	C−N						N−N			
	covalent				weak coupling		folding		collinear	
	1A1	1A2	1A3	1A4	1B1	1B2	2A1	2A2	2B1	2B2
C_1	0.005	0.005	0.005	0.006	0.389	−0.010	0.213	0.217	−0.028	−0.028
N_2	0.019	0.019	0.022	0.023	−0.090	0.234	−0.035	−0.048	0.488	0.488
N_3	0.000	0.000	0.000	−0.001	−0.075	0.005	−0.042	−0.038	0.008	0.008
C_4	0.004	0.004	0.018	0.018	0.361	−0.002	0.114	0.120	−0.009	−0.009
C_5	−0.007	−0.007	−0.013	−0.013	0.217	0.005	0.281	0.281	0.019	0.019
C_1'	0.005	0.005	0.444	0.446	−0.011	0.390	0.213	0.217	−0.028	−0.028
N_2'	0.377	0.377	−0.135	−0.136	0.237	−0.090	−0.035	−0.048	0.488	0.488
N_3'	0.113	0.113	0.046	0.047	0.002	−0.076	−0.042	−0.038	0.008	0.008
C_4'	−0.056	−0.056	0.632	0.633	−0.001	0.356	0.114	0.120	−0.009	−0.009
C_5'	0.529	0.529	0.001	−0.002	0.011	0.227	0.281	0.281	0.019	0.019

[a] The spin densities over all H centers are basically equal to zero, thus are omitted.

TABLE 6: Mulliken Charge Populations of Single and Double H-Bond Modes Complexes Determined at B3LYP/6-311+G* Level

	single H-bond								
	C−H···N				N−H···N		double H-bond		
	3A1	3A2	3A3	3A4	3B1	3B2	4A	4B	4C
C_1	−0.080	−0.075	−0.303	−0.330	−0.079	−0.188	−0.096	−0.097	−0.180
N_2	−0.061	−0.055	−0.065	−0.054	−0.389	−0.051	−0.111	−0.131	−0.094
N_3	−0.214	−0.223	−0.214	−0.208	−0.264	−0.220	−0.246	−0.246	−0.241
C_4	−0.116	−0.173	−0.074	−0.070	−0.130	−0.146	0.139	0.124	−0.112
C_5	−0.329	−0.278	−0.150	−0.149	−0.218	−0.154	−0.532	−0.558	−0.211
H_6	0.292	0.293	0.401	0.405	0.295	0.263	0.277	0.274	0.316
H_7	0.460	0.461	0.451	0.450	0.480	0.672	0.457	0.459	0.461
H_8	0.289	0.290	0.284	0.284	0.289	0.278	0.321	0.324	0.271
H_9	0.466	0.479	0.295	0.295	0.295	0.267	0.292	0.292	0.290
C_1'	−0.115	−0.116	−0.105	−0.118	−0.189	−0.079	−0.096	−0.152	−0.180
N_2'	−0.241	−0.252	−0.200	−0.194	−0.050	−0.389	−0.111	−0.068	−0.094
N_3'	−0.241	−0.242	−0.235	−0.237	−0.219	−0.264	−0.246	−0.236	−0.241
C_4'	−0.041	−0.037	−0.036	−0.058	−0.145	−0.132	0.139	−0.115	−0.112
C_5'	−0.319	−0.322	−0.313	−0.276	−0.155	−0.217	−0.532	−0.204	−0.211
H_6'	0.258	0.259	0.264	0.264	0.263	0.295	0.277	0.311	0.316
H_7'	0.453	0.456	0.452	0.450	0.672	0.480	0.457	0.458	0.461
H_8'	0.258	0.255	0.266	0.262	0.278	0.289	0.321	0.274	0.271
H_9'	0.280	0.280	0.283	0.283	0.267	0.295	0.292	0.291	0.290

(**I**)−C_5(**II**) is 1.533 Å, just equal to that of 1A3. The difference mainly lies in the **II** moiety, which can be seen easily from Figure 2. The angle of $\angle N_2$(**I**)−C_5(**II**)−H_6(**II**) is 103.6°, equal to the corresponding angle of 1A3, while the angles of $\angle N_2$(**I**)−C_5(**II**)−N_3(**II**) and $\angle N_2$(**I**)−C_5(**II**)−H_4(**II**) of 1A4 are almost equal to the corresponding angles of 1A3 either. These phenomena indicate that the effect of the rotation on 1A3 is smaller. It can be concluded from the dipole moments of these four complexes given in Table 8 that they all possess notable polarity.

The vibrational spectra are strongly influenced by the formation of the complex compared to those of the monomers. It can be seen from Figure 3 that the vibrational frequencies of 1A1 and 1A2 with notable IR intensities densely distribute in the fingerprint section. There are two vibrational modes with very strong IR intensities around 3600 cm^{-1}, they are the typical

TABLE 7: Spin Densities (ρ) of Single and Double H-Bond Mode Complexes Obtained at B3LYP/6-311+G* Level[a]

	single H-bond						double H-bond		
	C−H···N				N−H···N				
	3A1	3A2	3A3	3A4	3B1	3B2	4A	4B	4C
C_1	0.329	0.330	0.281	0.282	0.000	0.507	0.205	0.187	0.215
N_2	−0.073	−0.072	−0.050	−0.050	0.001	−0.105	−0.048	−0.049	−0.029
N_3	−0.056	−0.057	−0.045	−0.045	0.000	−0.094	−0.030	−0.025	−0.040
C_4	0.242	0.241	0.190	0.192	0.000	0.354	0.169	0.166	0.126
C_5	0.343	0.348	0.281	0.327	0.000	0.406	0.236	0.222	0.259
C_1'	0.110	0.111	0.147	0.141	0.507	0.000	0.205	0.228	0.215
N_2'	−0.023	−0.021	−0.028	−0.029	−0.104	0.000	−0.048	−0.036	−0.029
N_3'	−0.019	−0.019	−0.026	−0.023	−0.094	0.000	−0.030	−0.040	−0.040
C_4'	0.081	0.078	0.100	0.104	0.353	0.000	0.169	0.142	0.126
C_5'	0.130	0.127	0.170	0.165	0.407	0.000	0.236	0.267	0.259

[a] The spin densities over all H centers are basically equal to zero, and thus are omitted.

TABLE 8: Dipole Moment (DM, in D), Stabilization Energies (E_s, in kcal/mol) and E_s* (after Correction) of the Complexes Obtained at B3LYP/6-311+G* Level

	1A1	1A2	1A3	1A4	1B1	1B2	2A1	2A2	2B1	2B2
DM	3.973	3.973	7.544	7.487	2.776	4.356	0.001	1.268	1.599	1.610
E_s	35.0	35.0	29.5	29.5	26.6	26.5	25.1	26.0	23.6	23.6
E_s*	30.2	30.2	25.7	25.7	24.0	23.7	22.5	23.3	20.8	20.8

	3A1	3A2	3A3	3A4	3B1	3B2	4A	4B	4C
DM	3.407	3.386	3.223	2.656	7.573	7.563	0.001	1.678	0.003
E_s	22.5	22.3	22.6	22.5	37.6	37.6	22.9	23.5	24.3
E_s*	21.3	21.2	21.5	21.4	35.7	35.6	21.8	22.2	23.0

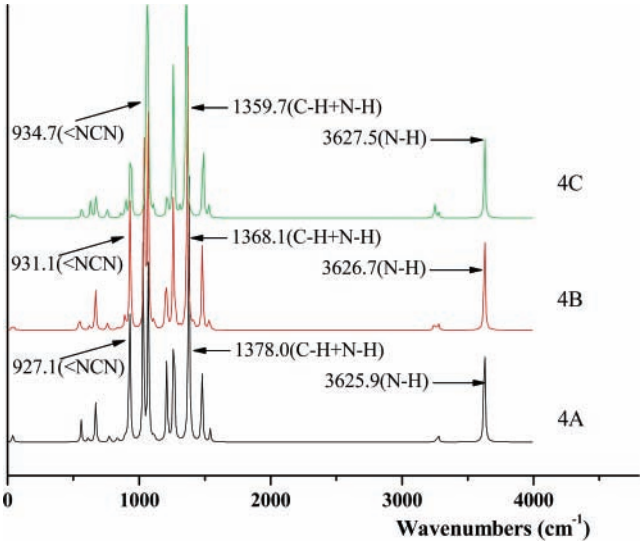

Figure 7. IR spectra of the double H-bond coupling mode obtained at the B3LYP/6-311+G* level.

stretching vibrations of N−H bond. At 496.1 and 1080.2 cm^{-1}, there are strong IR absorptions, being sway out of the plane of N−H (**II**) and stretching of N_2(**I**)−C_1(**II**), but the corresponding vibrational modes are red-shifted compared with the corresponding modes of the monomers (see Table 2). The other aspect which can be seen is that a vibrational peak around 3000 cm^{-1}, being assigned as the C_1−H_6 stretching of **II**, is red-shifted by >200 cm^{-1} compared with the monomers. The conclusion can be drawn that the interaction strength of C_1−H_6 is weakened due to the combination of N_2(**I**)−C_1(**II**). The configuration of 1A3 is similar to that of 1A1. The distinct characteristic of 1A3 compared with 1A1 is that the frequency of the N−H (**II**), sway out of plane, is red-shifted compared with Im by 57.3 cm^{-1}. At 1077.8 cm^{-1} is the other absorption peak with strong IR intensity, which denotes the sway of N_2-(**I**)−C_5(**II**). There are two vibrations over 3600 cm^{-1} with strong IR intensities (3621.2 and 3632.3 cm^{-1}), and they denote the stretching of two N−H bonds. The vibration of $\upsilon_{C_5-H_9(II)}$ is red-shifted by 240.8 cm^{-1} compared with Im^+ (see Table 2). It can be seen that the configuration of 1A4 is similar to that of 1A3, and the frequency analyses indicate that the vibrational modes of these two complexes are also very similar to each other. The interaction between two fragments in each of these four complexes causes the redistribution of electrons compared with the monomers (Im and Im^+). Therefore, the electron density of one fragment is increased, while the electron density of the another is decreased, viz. the electron transfer from Im to Im^+ moieties, causing the bonding interaction of each fragment change. Obviously, this analysis can be used in interpreting such a fact that one N−H bond is red-shifted while the other N−H bond is blue-shifted spectroscopically.

Table 4 has collected the total Mulliken atomic charges of these complexes. For 1A1 and 1A2, most of the negative charges of **I** mainly locate on N_3 and C_5 positions, while N_2 carries significantly positive charge. For the **II** fragment, the negative charges mainly centralize on C_1 (−0.777) atom which contacts with N_2 (carrying notable positive charge) of **I** directly. It is easy to understand that such a distribution should always lower the total energy of a radical system. Another phenomenon is that almost all of the positive charges (96.1%) of the molecule distribute over **I**. Therefore, it can be judged from the above analyses that **I** has been oxidized by **II**. Similar to the distribution of 1A1, the charges of **I** fragment of 1A3 also mainly distribute on N_3 and C_5 atoms, and there are more positive charges centralizing on N_2 atom. The direct contact atom of **II** is C_5 instead of C_1. It also can be seen that almost all of the charges locate on **I**. The similar conclusion can be drawn that the complex should be regarded as Im(**I**)−Im^+(**II**) molecule. The structure similarity actually reflects the charge population similarity between 1A3 and 1A4. This can be verified by the data listed in Table 4.

The spin density distribution of this mode should be distinct for its covalent coupling. It can be seen from Table 5 that most of the spin densities of 1A1 and 1A2 are localized on N_2, N_3,

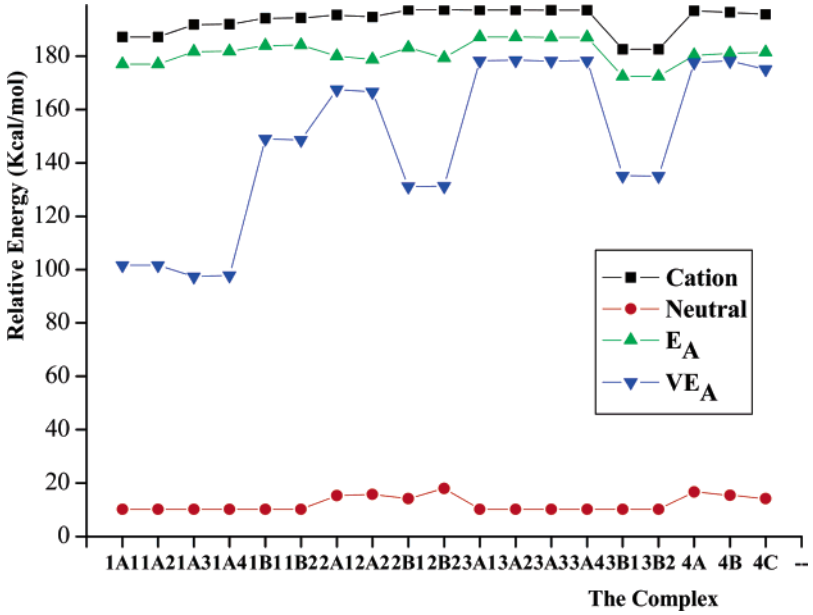

Figure 8. Relative energies of the complexes obtained at the B3LYP/6-311+G* level on the basis of the same zero point.

and C_5 positions of **II**, which is different from those of the monomers (Table 3). And it should also be mentioned that the other moiety (**I**) only carries a little amount of spin density in the complex. Thus, instead of sharing any spin density with **II**, the role of **I** is mainly to delocalize the spin single electron from N_2 at the rest atoms of **I**. It has been mentioned in ref 20 that, in general, such a spin delocalization should lower the energy of the system. The result of this strong spin delocalization effect is that the spin density of C_1 redistributes on two approaching N atoms. The situation of 1A3 is similar to that of 1A1. Most of the spin densities are mainly located on C_1 and C_4 positions of **II**, while **I** still keeps the characteristics of the free Im. The ρ distribution of 1A4 is similar to that of 1A3. This can be verified by the data collected in Table 5.

The second C···N mode is the C···N weak coupling one, which includes two complexes. From Figure 2, it can be easily seen that the coupling mode 1B1 is similar to 1B2, two fragments interact with each other through C···N weak interaction, and at the same time two fragments almost lie in two perpendicular planes. The most notable difference between these two complexes is that one of two fragments rotates 180.0° by keeping another fragment fixed. The contact distances of two parts of these two complexes are 2.225 and 2.233 Å, respectively, and the difference between them is 0.008 Å. The atoms of each fragment still keep in coplane, similar to Im. Their corresponding dipole moments (DM) are 2.776 and 4.356 D, respectively.

Figure 3 has shown that most of the vibrational spectra with strong infrared intensities of 1B1 also distribute in the fingerprint section. The vibrational mode with very strong IR intensity lies above 3600 cm^{-1}. Actually, this absorption peak includes two vibrational modes, and their frequency difference is small (5.6 cm^{-1}), and therefore, it looks undistinguishable for these two frequencies. These two vibrational modes denote the stretching vibrations of N−H bonds. It is clear that there are two distinguishable frequencies above 3600 cm^{-1} for 1B2, although its most characteristics are similar to those of 1B1. It also should be noted that there are vibrations around 3260 cm^{-1} for each of these five complexes and the frequency analyses tell us that these vibrational modes correspond to the stretching of C−H bonds.

The Mulliken atomic charge populations of these two complexes are also given in Table 4. It can be seen from this table that the charges of 1B1 and 1B2 almost equally distribute in two fragments. For the **I** fragment of 1B1, the negative charges mainly distribute among C_1, N_3, C_4, and C_5 atoms, while for the **II** fragment, the negative charges mainly distribute among C_1, N_3, and C_5 atoms. For 1B2, the charges equally distribute over two fragments. The negative charges of **I** mainly distribute over N_3 and C_5 atoms, while the charges of N_2 and C_4 are positive. The negative charges of **II** mainly distribute among all C and N atoms except N_2.

The spin densities (ρ) of the complexes obtained at the B3LYP/6-311+G* level are listed in Table 5. For this coupling mode, there is no direct contact between two fragments and the coupling effect on each other is small; therefore, their ρ should still carry the characteristics of the monomers. Similar to the spin density distribution of Im^+, ρ of **I** in 1B1 also mainly centralizes on C_1, C_4, and C_5 atoms, while interestingly, the **II** moiety does not carry any significant amount of spin density in the complex. Thus, 1B1 can be regarded as the Im^+(**I**)···Im(**II**) complex. For 1B2, the situation is just inverse; almost no spin density localizes on the **I** moiety, and ρ of **II** mainly centralizes on the C_1, C_4, and C_5 atoms. Therefore, this complex can be taken as the Im(**I**)···Im^+(**II**) complex.

3.2. N···N Mode. The N···N coupling mode also consists of two distinct (folding and collinear) modes. Two fragments are parallel to each other for each folding mode complex, while for the collinear mode, two fragments are arranged in a line and in two almost perpendicular planes. There are two complexes for each of two modes; they are 2A1 and 2A2 for the N···N folding mode and 2B1 and 2B2 for the N···N collinear mode, respectively.

Figure 2 indicates that the interaction mode of 2A1 is similar to that of 2A2. The position of two fragments is parallel to each other. The most distinct difference of 2A2 compared with 2A1 lies in that one fragment rotates 180.0° along the axis which parallels with the C−C bond by keeping the other fragment fixed. The contact distances of these two complexes are 3.215 and 3.092 Å, respectively, and their difference is notable. The atoms of each fragment still keep in one plane. Their corresponding DMs are 0.001 and 1.268 D, respectively. It indicates

that two parts of 2A1 are symmetrical and the electrons are equally distributed, while the 2A2 carries polarity.

The spectrum characteristics of 2A1 and 2A2 are different from those of 1B1 and 1B2 although most of the vibrational frequencies with strong IR intensities also distribute in the fingerprint section. For 2A1, the vibrational frequency with the strongest IR intensity is 1370 cm^{-1}, which is stronger than that of ~3600 cm^{-1} and denotes the hybrid sway of C−H and N−H bonds. The primary vibrational modes are assigned in Figure 4. The spectrum characteristics of 2A2 are similar to those of 2A1. The IR intensity of 1370 cm^{-1} also is the strongest among the frequencies of 2A2, and even stronger than the corresponding one of 2A1. The vibrational mode of the frequency about 3600 cm^{-1} also denotes the N−H stretching.

Two fragments of 2A1 are parallel to each other. The charges of 2A1 symmetrically distribute in two fragments, and the negative charges mainly distribute among C_1, N_3 and C_5 atoms, as shown in Table 4. The charge distribution of 2A2 is similar to that of 2A1 except that not much charge locates on the N_4 position.

Table 5 reveals that the ρ distributions of two fragments of each complex for 2A series are seen to be equal to each other and mainly locate on three C atoms (C_1, C_4, and C_5), similar to the spin distribution of Im^+. Thus, one still needs other information (such as bonding and charges distribution) if judging the composition of these two complexes. The other point that should be noted is that the ρ distribution of 2A2 is similar to that of 2A1.

The other N···N coupling mode is the N···N collinear one. For 2B1 and 2B2, they are actually two distinct structures, and their difference can easily be seen from Figure 2, though their contact distances and the stabilization energies are equal to each other no matter whether considering the ZPE and BSSE corrections or not. The difference of these two geometries mainly lies in the position of fragments. In other words, if **I** fragment of 2B1 rotates around the N···N axis by 180.0° and at the same time **II** fragment is fixed, the geometry structure of 2B2 comes into being. The atoms of each fragment are in one plane, and the dihedral of these two planes is close to 90.0°. This is the same characteristic of these two complexes. These two complexes can be viewed as the image isomers. The contact distance of two fragments in 2B1 is equal to that in 2B2, about 2.147 Å.

Similar to the former complexes, most of the vibrational frequencies with strong infrared absorption intensities of 2B1 and 2B2 distribute in the fingerprint section. The character of the vibrational spectrum of 2B2 is similar to that of 2B1. The vibrational modes of ~3600 cm^{-1} denote the stretching of the N−H bonds. There is one common phenomenon for these complexes, which is that one N−H bond is blue-shifted spectroscopically for each of them while another N−H bond is red-shifted. This observation should be due to the interaction of two fragments; therefore, the electrons redistribute in two fragments, leading to the strengthening of the N−H bond of Im^+ and the weakening of the N−H bond of Im cooperatively. It also indicates the composition of the complexes; therefore, the results obtained from the spin density can be also verified.

The structures of 2B2 and 2B1 are different, but the charge population of 2B2 is similar to that of 2B1. The charges symmetrically locate over two fragments, and the negative charges symmetrically distribute over C_1, N_3, and C_5 atoms, respectively. Some positive charges locate on the N2 position, while H_7 (and H_7') also carries most of the positive charges.

The spin density equally distributes over two fragments in 2B1. The richest sites are N_2 and N_2' (0.488) sites, and ρ over the other atoms are near zero, much more like that of Im. The ρ values of 2B2 and 2B1 are similar to each other. These can be verified by the data in Table 5.

3.3. Single H-Bond Mode. It is well-known that the H-bond plays a key role in chemistry, physics, and biology. This kind of intramolecular and intermolecular hydrogen bond also plays a role in protein folding and the binding between some nucleoside bases.[21−22] Two features are common to all generally accepted variants of H-bonds: one is a significant charge transfer from the proton acceptor (Y) to the proton donor (X−H) and another is the weakening of the X−H bond due to the formation of the X−H···Y H-bond. This weakening is accompanied by the bond elongation and a concomitant red shift of the X−H stretch vibrational frequency compared to the noninteracting species. Generally speaking, the character of the X−H···Y type H-bond may be described as follows: (1) the X−H covalent bond stretches in correlation with the strength of the H-bond; (2) a small amount of electron density is transferred from the proton acceptor (Y) to the proton donor molecule; (3) the band which corresponds to the X−H stretching shifts to the lower frequency (red shift), increases in intensity, and broadens.[23] Two fragments of this coupling mode complex interact through the C−H···N or the N−H···N type H-bond. Only a few papers about the N−H···N[11,13,15,24,25] type H-bond have been published until now. Therefore, it is necessary and important to study Im in detail. The optimized geometry structures of this mode are also drawn in Figure 2, the harmonic vibrational frequencies are expressed in Figure 5, and the Mulliken charge populations (Q) and the spin densities (ρ) are expressed in Table 6 and Table 7, respectively. The PESs of the proton transfer are depicted in Figure 6.

Four complexes which contain C−H···N type H-bond are found. Figure 2 indicates that 3A1 and 3A2 and also 3A3 and 3A4 can be viewed as the image isomers, respectively, and the main difference of 3A1 from 3A3 lies in the atoms participating in the H-bonds. For 3A1 and 3A2, the C_5-H_9(**I**) group and N_2(**II**) atom participate in the forming of the C−H···N type H-bond, and three atoms of the H-bond are collinear. While the C_1-H_6(**I**) group and N_2(**II**) atom participate in the forming of the C−H···N type H-bonds of 3A3 and 3A4, the angles of three atoms of the H-bond are 166.1 and 168.2, respectively. The contact distance of two fragments is also different, and they are 2.140 and 2.148 Å for 2A1 and 2A2 and 2.213 and 2.203 Å for 2A3 and 2A4, respectively. The contact distances of 3A3 and 3A4 (C_1(**I**)−N_2(**II**)) are 3.279 and 3.275 Å, larger than the corresponding contact distances (3.231 and 3.238 Å) of 3A1 and 3A2. Therefore, these four hydrogen bonds should belong to the weak hydrogen bonds for their large contact distances.

Most of the vibrational frequencies with strong infrared absorption intensity also distribute in the fingerprint section. There are two frequencies (1061 and 1372 cm^{-1}) with very strong IR intensity. The frequency analyses have assigned them to be scissors of C_4-H_8 and C_5-H_9 bonds and sways of C_5-H_9, C_4-H_8, and N_3-H_7 bonds, respectively. The other main difference is that the absorption peaks of the two 3600 cm^{-1} modes are small. The two fragments of this mode conformation interact through the C−H···N H-bond. The corresponding frequencies of this H-bond are ~3090 cm^{-1} for 3A1 and 3A2, which are red-shifted compared with the corresponding frequency of Im^+, but the IR intensity increases. The vibrational modes of 3A3 and 3A4 are similar to those of 3A1 and 3A2. Two fragments of this complex interact by different C−H···N

H-bond, and the frequency of this H-bond is ~3155 cm^{-1}, which is also red-shifted. These hydrogen bonds are red-shifted compared with those of the corresponding of Im^+ by about 170 and 110 cm^{-1}, respectively.

Similar to the phenomenon of the covalent C−N coupling mode, there is a vibrational peak around 3100 cm^{-1}, and it denotes the red-shifted stretching of C−H bonds. However, their mechanisms are distinct completely. For the covalent C−N coupling mode, the weakening of C−H bond is the result of the forming of the C−N covalent bond, while the red-shift of the vibrational frequency of C−H bond can be taken as a result of the forming of the C−H···N bond for the complexes of the single H-bond mode.

There exists one C−H···N type H-bond for each complex of this coupling mode; therefore, it may be possible that the Mulliken charges distribute asymmetrically in two fragments, because it is convenient for the electron passing or transferring through the H-bridge (H-bond). For 3A1 and 3A2, the Mulliken charges mainly distribute over **I** fragment, and the proportion of charges between **I** and **II** is 7:3. Therefore, this complex can actually be regarded as Im^+(**I**)···Im(**II**) molecule. The negative charges of 3A3 and 3A4 mainly distribute on C_1, N_3, and C_5 of **I** and C_1, N_2, N_3, and C_5 of **II**. Table 6 also reveals that more than 60% of charges are located on the **I** fragment. The conclusion can be drawn that this complex can also be taken as Im^+(**I**)···Im(**II**) molecule.

For 3A1 and 3A2, as shown in Table 7, the ρ distribution of **I** mainly locates on three carbon atoms, which is similar to the ρ distribution of the imidazole cation. The ρ distribution of **II** also possesses the characteristics similar to the imidazole cation. Compared with **I**, the difference of **II** moiety with Im^+ is bigger. Therefore, 3A1 and 3A2 can be regarded as the Im^+(**I**)···Im(**II**) complex molecules. The ρ distribution of 3A4 is similar to that of 3A3, and they can be also regarded as Im^+(**I**)···Im(**II**) complexes.

It is the prominent characteristic that two fragments of 3B1 and 3B2 interact with each other via the N−H···N type H-bond. The atoms of these two H-bonds are collinear, similar to that of 3A1/3A2. The other remarkable character of these two geometries is that the proton transfer exists. This phenomenon also occurs in the imidazole−imidazolium system and has been discussed previously[15] by Tatara et al., but the mechanism is still unclear. The most notable difference of the structures of 3B1 and 3B2 lies in the cross orientation of two fragments. The contact distance (N−H···N) of two fragments after the proton transfer is almost equal to each other, 2.788 Å for 2B1 and 2.789 Å for 2B2. The essential difference is that the proton transfer is from N3 (**II**) to N2 (**I**) for 2B1, and that is from N3 (**I**) to N2 (**II**) for 2B2. Therefore, they can be viewed as the image isomers.

The frequencies of 3B1 are different from those of the formers demonstrated in Figure 5, and the IR intensity of 2721.8 cm^{-1} is very large. Frequency analysis has confirmed that this frequency refers to the N−H stretching of the N−H···N H-bond, but it is red-shifted grievously. The conclusion can be drawn that the coupling interaction of two fragments should be very strong. The other N−H vibration is also red-shifted by 22.9 cm^{-1} compared with the corresponding one of Im. The spectroscopic character of 3B2 is similar to that of 3B1.

The Mulliken charge distribution of 3B1 is distinct with that of the former complexes for the proton transfer. There are about 27.9% of the positive charges locating on **I**, while the H_7' atom transfers from **II** to **I** moiety. Furthermore, if taking the proton transfer into account, there are about 95.1% of the positive charges locating on **I** moiety. Thus, this complex can be regarded as the Im(**I**)···Im^+(**II**) complex. There are notable negative charges on N_2 (−0.389) of **I** and N_3 (−0.219) of **II,** and the positive charge of H atom between these two atoms is 0.672. As known, such a charge distribution should always stabilize the system. The charge distribution of 3B2 is similar to that of 3B1. The negative charges mainly distribute among C_1, N_3, C_4, and C_5 of **I** and N_2, N_3, C_4, and C_5 of **II**. The most distinct character of this complex is that a proton transfers from **I** to **II**, being inverse in 3B1.

Most of the spin densities of the 3B1 actually locate on C_1, C_4, and C_5 positions of **II**. But for the **I** fragment, only the N_2 position carries a small amount of spin density, and the spin densities of the other four positions are basically zero. All of the spin densities of 3B2 actually locate on C_1, C_4, and C_5 positions of **I**, and the **II** moiety does not carry any spin density in the complex at all. Therefore, this complex can be regarded as the typical Im^+(**I**)···Im(**II**) molecule. This conclusion is also in accordance with that drawn from the Mulliken charge analysis.

The proton-transfer PESs of 3B1 and 3B2 are drawn in Figure 6. For 3B1, the surface denotes the proton-transfer process of H_7' from Im^+(**II**) to Im(**I**). In this course, it is very easy for the system to fall into a potential well (which depth is about 10 kcal/mol) after surpassing a small potential energy barrier (about 1.2 kcal/mol). Another point should be mentioned that the complex containing the N−H···N type H-bond but without proton transfer is not found. Therefore, it can be concluded that this proton transfer reaction is almost a spontaneous process, and the potential barrier is at the critical boundary from existing to disappearing. The characteristics of the proton transfer of 3B2 is similar to 3B1, the difference mainly lies in that **I** denotes the Im^+ molecule fragment while **II** expresses the Im molecule fragment; thus, the H_7 atom of **I** transfers to **II**, instead of H_7' transfer of **II** to **I**. This reaction should also be spontaneous. The conclusion can be drawn that this process is a proton transfer from Im^+ to Im instead of the hydrogen-atom transfer. It is possible that the electron can be transferred by N−H···N H-bond. Therefore, these two equilibrium structures are used as the starting geometries in the optimizations of the neutral complexes. It is found that no notable proton or hydrogen transfer occur for the corresponding neutral complexes. Thus, the conductivity in imidazole chains is likely to be due to proton traverse between two adjacent imidazole rings. Namely, the proton transfers to the other moiety when one electron is removed from the neutral complex, and when one electron is added on the complex of Im and Im^+, the proton goes back to the Im^+ moiety. This mechanism is in accordance with that proposed in ref 5. The ionization process from the neutral complex should thus correspond to the rate-limiting step for the protonic conductivity in imidazole chains. The calculated ionization energies of two neutral complexes at B3LYP/6-311+G* are about 185.4 kcal/mol.

The diffusion mechanism of an excess proton in imidazole molecule chains has been studied using the CPMD code.[26] In that case the proton transfer was found to be coupled to the reorientation step, which is the rate-determining step as mentioned in ref 5. The barrier for proton transfer between Im and ImH^+ has been calculated,[16] but no complete geometry optimization was done at that time. This proton-transfer process has been studied in ref 15, and it indicated that the proton transfer potential energy curve has a broad double well shape with a very small energy barrier. At the room temperature the proton can move freely from one side to the other. This is in

accordance with our calculations that the proton transfers spontaneously at room temperature.

3.4. Double H-Bond Mode. Each complex contains two C−H···N type H-bonds, which is the most distinct characteristic of the double H-bond mode complexes. Figure 2 reveals that each fragment of 4A interacts with the other part through similar atoms. In other words, N_2 and C_4-H_8 of **I** interact with H_8-C_4 and N_2 of **II**, cooperatively forming two C−H···N type H-bonds ($C_4-H_8\cdots N_2$). The N···H contact distances of these two H-bonds are equal to each other, 2.555 Å, being the longest among all the H-bonds. The angle of $C_4-H_8\cdots N_2$ is about 134.5°. If one substitutes the C_4-H_8 group of **II** with the C_1-H_6 group, namely, rotating **II** around the line through N_2 and ring **II** center and keeping **I** fixed, the structure of 4B can be obtained. Two H-bonds in this rotamer are $C_4-H_8\cdots N_2$ and $C_1-H_6\cdots N_2$, and the angles of $C_4-H_8\cdots N_2$ and $C_1-H_6\cdots N_2$ are 133.1 and 132.0°, respectively. The N···H contact distances of these two H-bonds are 2.504 and 2.464 Å, respectively, shorter than those of 4A. If two C_1-H_6 groups participate in the forming of H-bonds instead of two C_4-H_8 groups, the configuration of 4C is obtained. There are two C−H···N type H-bonds ($C_1-H_6\cdots N_2$) in this structure, and the N···H contact distance of these two H-bonds are 2.423 Å, equal to each other, being the shortest among these three rotamers. The angle of $C_1-H_6\cdots N_2$ is about 129.3°, also the smallest among these H-bonds. The conclusion can be drawn that the combining strength of 4C should be stronger than that of 4B, to say nothing of 4A.

The IR spectra of double H-bond coupling mode complexes are drawn in Figure 7. Most of the frequencies with strong IR intensities of 4A distribute in the fingerprint section. There also is a frequency with very strong IR intensity over 3600 cm^{-1}, but the strongest is at 1378 cm^{-1}, which denotes the asymmetrical sway of C_4-H_8 and N_3-H_7 bonds. It can be seen that the structures of 4A and 4B are similar. The most distinct difference lies in that the frequencies around 1000 cm^{-1} are red-shifted. The vibrational mode with the strongest IR intensity of 4B is the asymmetrical sway of C_4-H_8 and N_3-H_7 bonds. The vibrational frequencies with strong IR intensity of 4C located in fingerprint section are fewer compared with those of 4A and 4B. The most distinct character lies in that there are two frequencies with very strong IR intensity for these three complexes, which are 1069.1 and 1368.1 cm^{-1} for 4A, 1032.0 and 1378.0 cm^{-1} for 4B, and 1064.6 and 1359.7 cm^{-1} for 4C, respectively. The corresponding vibrational modes of these two frequencies are symmetrical or asymmetrical hybrid sways of all C−H and N−H bonds. One common phenomenon is that the frequencies of N−H bonds are almost equal to each other for each of three complexes; namely, one is red-shifted and the other is blue-shifted compared with the corresponding vibrational frequencies of the monomers. This phenomenon should be attributed to the electron redistribution, which can be seen from Table 6.

For each complex of the double H-bond coupling mode, its charge distribution is different from those of the formers. The structures of two fragments of 4A are similar to each other, and the charge population of two fragments is also similar to each other judging from Table 6. The negative charges mainly distribute over N_2, N_3, and C_5 centers of each fragments, and the effect of the notable negative charge located at N_2 (−0.111) and N_5 (−0.532) causes a distinct change of charge distribution at the C_4 center (0.139). It is different for 4B, which is not in symmetry at all. The negative charges of **I** mainly distribute over C_1, N_3, C_4, and C_5 centers, while for **II**, the negative charges mainly distribute over N_2, N_3, and C_5 atoms. More than half of the molecular charges distribute over the **I** fragment. The conclusion can be drawn that the complex should be the Im^+(**I**)···Im(**II**) formalism. The symmetry of 4C is similar to that of 4A, so the charge population of two fragments is also in symmetry. The negative charges of **I** mainly locate on C_1, N_3, C_4, and C_5 centers, and the same is true for the **II** moiety. The molecular charges of this complex equally locate on two fragments.

It can be seen from Table 7 that the spin densities of 4A equivalently locate on two fragments. The ρ distribution of each fragment localize on three carbon positions, which has the characteristic of Im^+. The ρ distribution of 4B is not in symmetry like 4A, but the spin densities of each fragment still mainly centralize on carbon centers. Another point should be noted is that the spin densities located on **II** are less compared with those located on **I**. The ρ distribution of 4C is similar to that of 4A. The common characteristic for the spin density distributions of these three complexes is that the spin densities locate on carbon centers.

3.5. Relative Stability. In the forming process of the complex from Im and Im^+, the total energy of the system is lowered. The energy difference between the total electronic energy of the complex and the sum of the total electronic energies of the monomers when they are isolated is defined as the stabilization energy, E_s. The bigger this value, the lower the system's energy and the more stable the system. There are two dominating factors that can affect the veracity of the stabilization energy, and they are ZPE and BSSE. Table 8 has listed the calculated stabilization energies of the complexes corrected with and without ZPE and BSSE.

It is helpful to analyze the interaction type between two fragments of each kind of complexes before the determinations of the stabilization energy. For four C···N covalent coupling mode complexes, the dominating contribution obviously is the covalent coupling interaction. The interaction of two fragments also involves the deformation of the monomers, the electrostatic attraction, and steric repulsion although these three types of interaction are small compared with the strength of the covalent bond. The effect of covalent bond, the deformation of the monomers, and the electrostatic attraction should always lower the energy of the system, while the effect of the steric repulsion should always increase the energy of the system. The stability of these four complexes is also enhanced by the polarization mechanism, which can be verified by the notable dipole moments expressed in Table 8. Thus, the total interaction of two fragments should be strong, and the complexes should be stable. For the C···N weak coupling mode complexes, the interaction between two fragments mainly includes the van der Waals attraction, the deformation of the monomers, and the electrostatic attraction. The effect of these three types of interactions should always lower the energy of the system. The stability of the C···N weak coupling mode complexes is also enhanced by the polarization mechanism. It also can be concluded that the energies of the C···N covalent coupling mode complexes should be lower than the energies of the C···N weak coupling mode complexes.

The interaction of N···N folding mode complexes mainly includes the van der Waals attraction and the electrostatic attraction. The composition of the interaction of N···N collinear mode complexes mainly includes the van der Waals attraction and the electrostatic repulsion, and the van der Waals attraction of two fragments is weaker compared with that of the N···N folding mode complexes. Therefore, the energies of the N···N folding mode complexes should be lower than the energies of

the N···N collinear mode complexes. It also can be inferred that the energies of the C···N covalent mode complexes should be lower than the energies of the N···N mode complexes. There are three types of interaction for the C···N weak coupling mode complexes and only two for the N···N folding mode complexes; however, the van der Waals attraction and the electrostatic attraction of the C···N weak coupling mode complexes are stronger than those of the N···N folding mode complexes. Therefore, it is difficult to judge which mode complex is energetically lower only through theoretical analysis.

The main interaction of the C−H···N type single H-bond mode complexes is the C−H···N type H-bond. While for the other single H-bond mode, the interaction consists of N−H··· N type H-bond and strong deformation of the monomers. Figure 6 has indicated that the energy of the system has been lowered following the deformation of the monomers, namely, the proton transfer from Im^+ moiety to Im. The dipole moments given in Table 8 also support that the stability of these complexes should be enhanced by the polarization mechanism. Therefore, it can be known that the energies of the N−H···N type single H-bond mode complexes should be lower than the energies of the other mode complexes. In addition, the energy of the C−H···N type single H-bond mode complexes should be lower compared with the energy of the N···N collinear coupling mode complexes.

There are two C−H···N type H-bonds for each of double H-bond coupling mode complexes. The binding strength of two fragments of each of double H-bond coupling mode complexes should be stronger compared with the interaction of two fragments of each of the C−H···N type single coupling mode complexes, and the double H-bond mode complexes should be energetically lower than the C−H···N type single H-bond mode complexes.

Thus, the conclusion about the stability of the system can be drawn with the above analyses, that is, the most stable coupling mode should be the N−H···N type single H-bond mode, and the N···N collinear coupling mode complexes should be higher energetically than the other modes, and the stability order of these coupling modes should be: 3B > 1A > 1B > 2A > 4 > 3A > 2B.

The calculated E_ss of 3B1 and 3B2 are 37.6 kcal/mol at the B3LYP/6-311+G* level, equal to each other, and bigger than the stabilization energies of other complexes. On the other hand, the interactions of two fragments of 3A1, 3A2, 3A3, and 3A4 are also through H-bonds, and their stabilization energies are 22.5, 22.3, 22.6, and 22.5 kcal/mol respectively, the smallest among all of these complexes. It can be seen from Table 8 that the E_s of the complexes of each coupling mode are almost equal except the single H-bond coupling mode. This may be caused by the effect of the ZPE. The stability order of these complexes after correction with the ZPE and BSSE methods is 3B1 > 3B1 > 1A1 = 1A2 > 1A3 = 1A4 > 1B1 > 1B2 > 2A2 > 4C >2A1 > 4B > 4A > 3A3 > 3A4 > 3A1 >3A2 > 2B1 = 2B2. This order is similar to the E_s tendency without correction. This observation is in good accordance with the above interaction type analyses. Another point also can be seen from Table 8 that the value of E_s* is smaller than E_s. In particular, for 1A1 and 1A2, the difference brought by the correction is about 4.8 kcal/mol, the biggest of all.

3.6. Electron Affinity. The electron affinity (E_A) is an important physical property of molecules and plays a vital role in electron-transfer reactions, and it is also helpful for the understanding of the electronic effect on system. E_As calculated using hybrid density functionals have been shown to be more accurate and to provide good agreement with the experimental values,[27−32] and these kinds of calculations have become well documented and established in recent years.[33,34] Thus, the calculated adiabatic E_As obtained using B3LYP method employing the 6-311+G* basis set for Im^+/Im in the present paper should also be accurate and reliable. In the convenience of comparison, the vertical electron affinities (VE_A) are also calculated at the same level of theory and are collected with the adiabatic electron affinities in Figure 8.

If the relative energies of the optimized Im^+···Im and the corresponding optimized neutral complexes are compared, the following several points can be drawn. The E_As of these cation complexes vary over a narrow range of values (∼180.0 kcal/mol). The most interesting result is the fact that, upon electron attachment, the stability order of 2A1 and 2A2 may alter. Configuration 2A2, which is more stable than 2A1 for the cation complex, is less stable than configuration 2A1 with the electron attachment, and the former has a higher dipole moment and a stronger interaction with the electron. As a result, the neutral configuration 2A2 has a slightly lower energy than configuration 2A1 by 0.5 kcal/mol. The other point can be seen is that the difference of the relative energies of the C···N mode complexes is reduced when the electron attached, while the difference of the relative energies of 2B1 and 2B2 is enhanced when the electron attachment. It can be also seen that the E_As of 3B1 and 3B2 are 172.4 kcal/mol, the smallest compared with the E_As of others, while the E_As of C−H···N H-bond mode complexes are the biggest, and bigger than those of 3B1 and 3B2 by ∼14.7 kcal/mol. It is generally known that the bigger the E_A is, the bigger the effect brought by the electron attachment to the complex is. Thus, when one electron is attached the electronic effects on the C−H···N H-bond mode complexes are the biggest, while that on 3B1 and 3B2 is the smallest. The VE_As of these cation complexes vary over a wide range of values, from 97.3 to 178.3 kcal/mol, but the difference of the VE_As for each type of the coupling mode complexes is small. The values of VE_As of the double H-bond mode complexes are almost equal to the corresponding E_As, which implies that the neutral complex at the optimized cation structure is near the corresponding optimized structure. Certainly, the notable difference of E_As and VE_As of three C···N covalent mode complexes indicates that the neutral complex at the optimized cation structure is far from the corresponding optimized neutral structure. Thus, the conclusion can be safely drawn that the deformation energies of the C···N covalent mode complexes should be the largest and the deformation energies of the double H-bond mode complexes should be the smallest.

4. Conclusions

On the basis of the reliable B3LYP/6-311+G* method, the structural character and relevant properties of the Im^+···Im coupling system have been explored in detail. Geometry optimizations have found four interesting coupling modes, and they may be classified as follows: the C···N coupling mode, the N···N coupling mode, the singlet H-bond mode, and the double H-bond mode. The C···N coupling mode consists of the C−N covalent coupling mode and the C···N weak interaction mode. The N···N coupling mode is composed by the folding and the collinear two typical coupling modes. The single H-bond mode may be characterized by the C−H···N and the N−H···N two types of H-bonds and for the double H-bond ones, there are two C−H···N type H-bonds in each of three double H-bond mode complexes. The IR spectra analysis indicates that most of the vibrations with strong IR intensity centralize in the fingerprint section. The primary vibrational modes are assigned

for all isomers. There are strong IR intensity absorption peaks over 3600 cm^{-1} (N−H stretching mode) for all of the complexes, except for the single H-bond (N−H···N) coupling mode complexes which is red-shifted grievously for the proton transfer. The proton transfer processes are investigated through the analysis of the PES. The positive charges of 1A, 3A and 3B mainly locate on their respective **I** moieties except for 3B1 which charges mainly locate on **II**, although those of other complexes locate equally on two fragments of each one. The spin density distribution analysis indicates that the characteristics of two fragments for each of 2A, 2B, 3A, 3B, 4A, and 4C are similar to each other. The complex composition can be safely determined with the combination of stable geometrical, frequency, Mulliken charges and spin density distribution analyses.

The interaction type analysis presents vital information for the stability of the complex. The calculated results of the stabilization energies indicate that 3B1 and 3B2 are two most stable complexes, while the E_s of 2B1 and 2B2 are the smallest; the energy difference between them (3B and 2B) after ZPE and BSSE corrections is about 14.9 kcal/mol. The E_s differences for the same coupling mode complexes are small. The adiabatic electron affinities indicate that the E_As of 3A series are the biggest while those of 3B series are the smallest among all complexes, implying the effect of the electron combination to be notable on 3A, but weak on 3B. It should be noted that the deformation energies of the C···N mode complexes from the stable cation structure to the corresponding optimized neutral geometry are the largest of all.

Actually, it is very possible there are various interaction modes among different biological fragments or the amino residues in the biological systems and the relevant processes, depending on the actual situation and the protein structure effect. The different coupling modes may yield different effect on the biomolecule structures and further regulate the functionality and reactivity mechanism of the relevant biological fragments. The key aspect of this work, taking Im and Im^+ ionic pair as example for its importance in biological systems, is to explore all possible interaction modes and to characterize such coupling structures in spectroscopy and energy, and so forth. Obviously, this work presents not only useful information for further investigations of this kinds of systems (such as about the isomerizations among different coupling modes, the proton conductivity, and the electron-transfer reactivity, etc.) but also an important clue for the approaches of other biological systems in theoretical aspects.

Acknowledgment. This work is supported by the National Natural Science Foundation of China (20273040) and the Natural Science Foundation of Shandong Province (Key project), and support from the SRFDP is also acknowledged.

References and Notes

(1) Sundberg, R. J.; Martin, R. B. *Chem. Rev.* **1974**, *74*, 471.
(2) Bachovchin, W. W. *Biochemistry* **1986**, *25*, 7751.
(3) Noguchi, T.; Inoue, Y.; Tang, X. S. *Biochemistry* **1999**, *38*, 399.
(4) Sorlie, M.; Christiansen, J.; Lemon, B. J.; Peters, J. W.; Dean, D. R. Hales, B. J. *Biochemistry* **2001**, *40*, 1540.
(5) Kawada, A.; McGhie, A. R.; Labes, M. M. *J. Chem. Phys.* **1970**, *52*, 3121.
(6) Colombo, L.; Bleckmann, P.; Schrader, B.; Schneider, R.; Plesser, Th. *J. Chem. Phys.* **1974**, *61*, 3270.
(7) Loeffen, P. W.; Pettifer, R. F.; Fillaux, F.; Kearley, G. J. *J. Chem. Phys.* **1995**, *103*, 8444.
(8) Su, Ch. Ch.; Chang, H. Ch.; Jiang, J. Ch.; Wei, P. Y.; Lu. L. Ch.; Lin, Sh. H. *J. Chem. Phys.* **2003**, *119*, 10753.
(9) Christen, D.; Griffiths, J. Z. *Naturforsch.* **1982**, *37a*, 1378.
(10) Perchard, C.; Novak, A. *J. Chem. Phys.* **1968**, *48*, 3079.
(11) Brédas, J. L.; Poskin, M. P.; Delhalle, J.; André, J. M.; Chojnacki. H. *J. Phys. Chem.* **1984**, *88*, 5882.
(12) Francisco, B. C.; Machado; Ernest, R.; Davidson *J. Chem. Phys.* **1992**, *97*, 1881.
(13) Scheiner, S.; Yi, M. Y. *J. Phys. Chem.* **1996**, *100*, 9235.
(14) Jalbout, A. F.; Adamowicz, L. *J. Phys. Chem. A.* **2001**, *105*, 1071.
(15) Tatara, W.; Wójcik, M. J.; Lindgren, J.; Probst, M. *J. Phys. Chem. A.* **2003**, *107*, 7827.
(16) Basch, H.; Krauss, M.; Stevens, W. J. *J. Am. Chem. Soc.* **1985**, *107*, 7267.
(17) Lee, C.; Yang, W.; Parr, R. G. *Phys. Rev. B* **1988**, *37*, 785.
(18) Frisch, M. J.; Trucks, G. W.; Schlegel, H. B.; Scuseria, G. E.; Robb, M. A.; Cheeseman, J. R.; Zakrzewski, V. G.; Montgomery, J. A.; Stratmann, R. E., Jr.; Burant, J. C.; Dapprich, S.; Millam, J. M.; Daniels, A. D.; Kudin, K. N.; Strain, M. C.; Farkas, O.; Tomasi, J.; Barone, V.; Cossi, M.; Cammi, R.; Mennucci, B.; Pomelli, C.; Adamo, C.; Clifford, S.; Ochterski, J.; Petersson, G. A.; Ayala, P. Y.; Cui, Q.; Morokuma, K.; Malick, D. K.; Rabuck, A. D.; Raghavachari, K.; Foresman, J. B.; Cioslowski, J.; Ortiz, J. V.; Stefanov, B. B.; Liu, G.; Liashenko, A.; Piskorz, P.; Komaromi, I.; Gomperts, R.; Martin, R. L.; Fox, D. J.; Keith, T.; Al-Laham, M. A.; Peng, C. Y.; Nanayakkara, A.; Gonzalez, C.; Challacombe, M.; Gill, P. M. W.; Johnson, B.; Chen, W.; Wong, M. W.; Andres, J. L.; Gonzalez, C.; Head-Gordon, M.; Replogle, E. S.; Pople, J. A. Gaussian, Inc., Pittsburgh, PA, 1998.
(19) Stephens, P. J.; Devlin, F. J.; Chabalowski, C. F.; Frisch, M. J. *J. Phys. Chem.* **1994**, *98*, 11624.
(20) Jiang, X.-K. *Acc. Chem. Res.* **1997**, *30*, 283.
(21) Jeffrey, G. A.; Saenger, W. *Hydrogen Bonding in Biological Structures*; Springer-Verlag: New York, 1994.
(22) Wahl, M. C.; Sundaralingam, M. *Trends Biochem. Sci.* **1997**, *22*, 97.
(23) Pavel, H.; Zden_k, H. *Chem. Rev.* **2000**, *100*, 4253.
(24) Chojnacki, H.; Lipinski, J. *Adv. Mol. Relax. Interact. Process.* **1980**, *18*, 149.
(25) Basch, H.; Krauss, M.; Stevens, W. J. *J. Am. Chem. Soc.* **1985**, *107*, 7267.
(26) Münch, W.; Kreuer, K. D.; Silvestri, W.; Maier, J.; Seifert, G. *Solid State Ionics* **2001**, *145*, 437.
(27) Boesch, S. E.; Grafton, A. K.; Wheeler, R. A. *J. Phys. Chem.* **1996**, *100*, 10083.
(28) Proft, F. de.; Geerlings, P. *J. Chem. Phys.* **1997**, *106*, 3270.
(29) Pak, C.; Xie, Y.; Van, Huis, T. J.; Schaefer, H. F., III. *J. Am. Chem. Soc.* **1998**, *120*, 11115.
(30) Richardson, N. A.; Wesolowski, S. S.; Schaefer, H. F. III. *J. Am. Chem. Soc.* **2002**, *124*, 10163.
(31) Zhan, Ch. G.; Nichols, J. A.; Dixon, D. A. *J. Phys. Chem. A* **2003**, *107*, 4184.
(32) Li, P.; Bu, Y. X.; Ai, H. Q. *J. Phys. Chem. A* **2004**, *108*, 1200.
(33) Rosch, N.; Trickey, S. B. *J. Chem. Phys.* **1997**, *106*, 8940.
(34) Oliveira, G. de.; Martin, J. M. L.; Proft, F. de.; Geerlings, P. *Phys. Rev. A* **1999**, *60*, 1034.